PHYSICAL REVIEW B **85**, 220103(R) (2012)

Tuning the range, magnitude, and sign of the thermal expansion in intermetallic $Mn_3(Zn, M)_x N (M = Ag, Ge)$

Cong Wang,[1,*] Lihua Chu,[1] Qingrong Yao,[2,3] Ying Sun,[1] Meimei Wu,[2,4] Lei Ding,[1] Jun Yan,[1] Yuanyuan Na,[1] Weihua Tang,[5] Guannan Li,[2,6] Qingzhen Huang,[2] and Jeffrey W. Lynn[2,†]

[1]*Center for Condensed Matter and Materials Physics, Department of Physics, Beihang University, Beijing 100191, People's Republic of China*

[2]*NIST Center for Neutron Research, NIST, Gaithersburg, Maryland 20899-6102, USA*

[3]*Department of Information Material and Engineering, Guilin University of Electronic Technology, Guilin 541004, People's Republic of China*

[4]*Department of Nuclear Physics, Chinese Institute of Atomic Energy, Beijing 102413, People's Republic of China*

[5]*State Key Laboratory of Information Photonics and Optical Telecommunications, School of Science, Beijing University of Posts and Telecommunications, Beijing 100876, People's Republic of China*

[6]*Beijing National Laboratory for Condensed Matter Physics, Institute of Physics, Beijing 100190, People's Republic of China*

(Received 8 February 2012; published 14 June 2012)

Neutron diffraction is used to reveal the origin and control of the thermal expansion properties of the cubic intermetallic compounds Mn_3Zn_xN and $Mn_3[Zn\text{-}(Ag,Ge)]_xN$. We show that the introduction of Zn vacancies induces and stabilizes an antiferromagnetic phase with huge spin-lattice coupling that can be tuned to achieve zero thermal expansion (ZTE) over a wide temperature range. We further show that the antiferromagnetic ordering temperature (T_N) that controls this ZTE can be tuned by chemical substitution, again on the Zn site, to adjust the span of ZTE temperatures from well above room temperature to well below. This establishes a quantitative relationship and mechanism to precisely control the ZTE of a single material, enabling it to be tailored for specific device applications.

DOI: 10.1103/PhysRevB.85.220103 PACS number(s): 65.40.De, 61.05.F−, 75.80.+q

Materials with negligible thermal expansion over large temperature ranges have been the subject of fundamental studies as well as being highly desirable for many modern technological applications, such as in spacecraft and for space telescopes,[1,2] thermomechanical actuators,[3] precision mechanics and positioning devices,[4] Bragg grating wavelength filters,[5] and microelectronic components. Presently the metallic materials of choice are Fe-Ni Invar-type alloys,[6,7] which generally have near-zero thermal expansion (NZTE) only near room temperature, but the temperature range for low thermal expansion recently has been extended to above 500 K by introducing stress, which produces microstrains around the Fe atoms.[8] ZTE materials avoid thermal strain in systems subject to large temperature variations, and thus have been a popular topic of longstanding focus.[9–13] It has been difficult to find new ZTE materials with metallic properties—most relatively new ZTE materials are ceramics[14–19]—but an exception has been found in manganese compounds Mn_3XB (X = Zn, Cu, Ni, Ge, ..., B = N and C),[20–28] because they may have isotropic ZTE, good electric and thermal conductivity, and other interesting physical properties. A clear guide on the origin of their thermal expansion behavior or how to control it is needed. In this Rapid Communication we use neutron powder diffraction (NPD) to uncover the origin of the isotropic zero thermal expansion of the cubic antiperovskite compounds $Mn_3(Zn/Ag/Ge)_xN$, focusing on the problem of how to control the temperature range of ZTE.

Polycrystalline samples of Mn_3Zn_xN ($x = 0.99, 0.96, 0.93$), $Mn_3Zn_{0.41}Ag_{0.41}N$, and $Mn_3Zn_{0.5}Ge_{0.5}N$ were prepared by a solid-state reaction in vacuum (10^{-5} Pa) using Mn_2N, Zn, Ag, and Ge as the starting materials. Stoichiometric amounts were mixed and pressed into pellets, wrapped in Ta foil, sealed in vacuum in a quartz tube, sintered at 800 °C for several days, and then cooled to room temperature. NPD data were collected in the 10–300 K temperature range on the BT-1 high-resolution neutron powder diffractometer at the NIST Center for Neutron Research using a Cu (311) monochromator (neutron wavelength of 1.5403 Å). Collimators of 15′, 20′, and 7′ were used before and after the monochromator and after the sample, respectively, and data were collected in steps of 0.05° in the 2θ range of 3°–168°. The temperature dependence of the nuclear and magnetic structures were determined by the Rietveld method with the General Structure Analysis System software, using scattering lengths of −0.375, 0.568, and $0.936(\times 10^{-12}\text{cm})$ for Mn, Zn, and N, respectively. Variable temperature x-ray diffraction data were also taken for the sample $Mn_3Zn_{0.5}Ge_{0.5}N$ from 110 to 580 K on a PANalytical X'Pert PRO powder diffractometer with a Cu target (wavelength 1.5406 Å). The sample was heated to the desired temperature at a rate of 10 K min^{-1} and held for 10 min. The x-ray diffraction (XRD) patterns at different temperatures were used to determine the lattice parameters. The crystal and magnetic structures of Mn_3ZnN, first reported by Fruchart *et al.*,[29,30] have Mn and N atoms forming Mn_6N octahedra, and Zn [at $1a(000)$] atoms on the corners of the cube, as shown in Fig. 1(c).

We first discuss the effect of Zn vacancies on the nature of the spin-lattice coupling by establishing the magnetic and structural properties for (refined) Zn site occupancies of $x = 0.99$, 0.96, and 0.93 (designated Zn99, Zn96, and Zn93; see Table I). All three compositions exhibit an identical antiferromagnetic ordering temperature of $T_N = 185$ K, below which a strongly first-order magnetic phase transition occurs at the magnetic structure shown in Fig. 1(b). The cubic structure

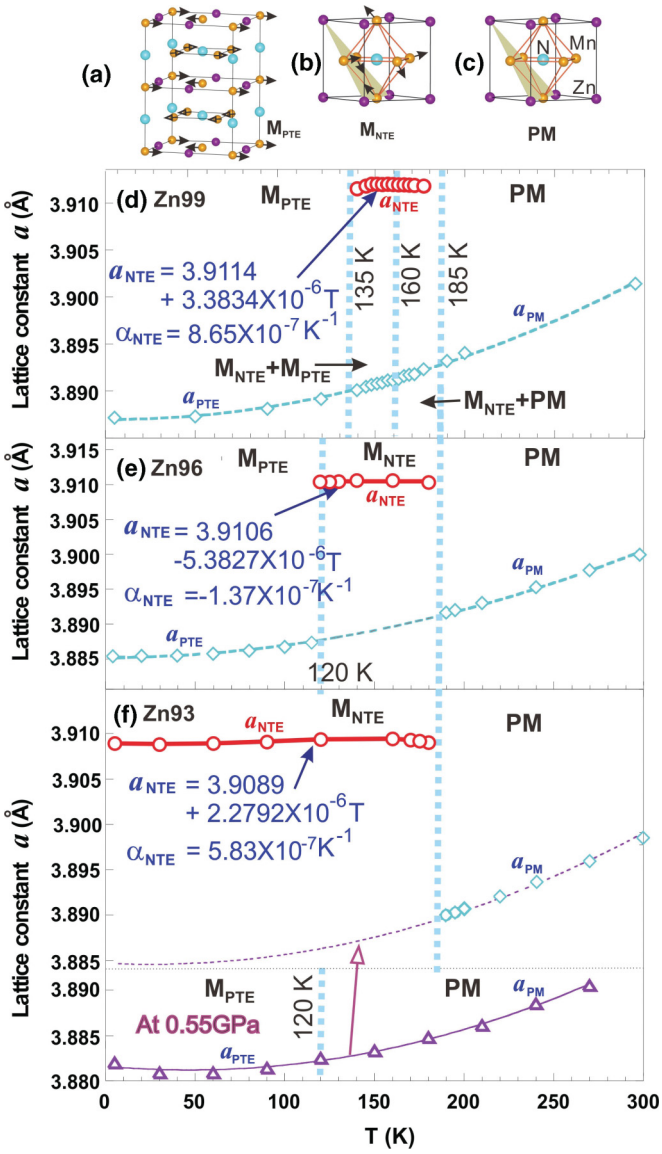

FIG. 1. (Color online) (a)–(c) Observed crystal and magnetic phases for Mn_3Zn_xN. (d)–(f) Temperature dependence of the cubic lattice constant for three values of Zn vacancies. All three samples are paramagnetic (PM) above 185 K with a cubic crystal structure. The M_{NTE} phase has the magnetic structure shown in (b), which for Zn99 is present between 185 and 135 K. (e) M_{NTE} temperature range is enlarged (185–120 K) for the Zn96 sample, with a complete PM to M_{NTE} transformation. The M_{PTE} phase is stable below 120 K. (f) For the Zn93 sample the M_{NTE} phase is stabilized in the entire temperature range below the PM-M_{NTE} transition at 185 K. In all three compounds the M_{NTE} phase has very small thermal expansion with $\alpha < 10^{-6}$ K^{-1}. An external pressure of 0.55GPa (△) converts M_{NTE} to M_{PTE}, or M_{PM} at higher T, where a_{PM} and a_{PTE} form the usual smooth curve observed in the Zn99 and Zn96 samples, without a detectable anomaly at the M_{PTE}-PM transition.

is maintained, but there is an abrupt increase in the lattice parameter for this phase, as shown in Figs. 1(d)–1(f) for Zn99, Zn96, and Zn93, respectively. This signals a strong negative thermal expansion at T_N, so we label this phase M_{NTE}. For the Zn99 composition only part of the sample transforms into the M_{NTE} phase, as shown in Fig. 2, with

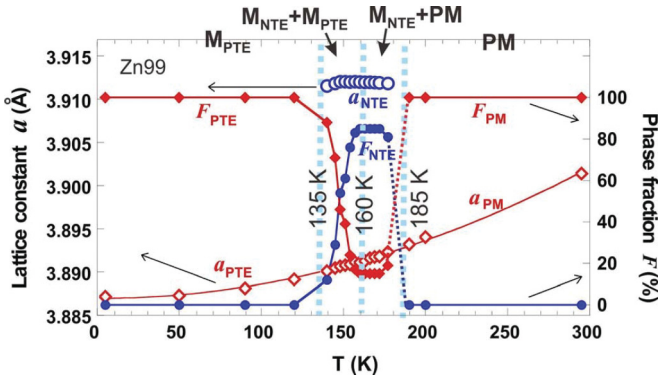

FIG. 2. (Color online) Relationship between the lattice variation and phase fractions for sample Zn99. The M_{NTE} phase is present between 185 and 135 K. The transition from PM to M_{NTE} is incomplete; an 83% M_{NTE} phase coexists with the PM phase between 185 and 160 K, and the M_{NTE} phase fraction decreases gradually on further cooling and coexists with the M_{PTE} phase between 160 and 135 K. Solid symbols represent phase fractions and open symbols depict lattice constants. Curves are guides to the eye.

the remainder of the sample initially remaining paramagnetic, and then transforming to the phase that exhibits a completely different magnetic structure shown in Fig. 1(a). The lattice parameter for this second magnetic structure follows the usual positive thermal expansion (PTE) and thus we designate this phase as M_{PTE}. We find that there exist two completely different antiferromagnetic (AFM) phases, with M_{NTE} having rhombohedral (R-3) magnetic symmetry while the M_{PTE} AFM phase has tetragonal ($P1$) symmetry. Only the M_{NTE} AFM displays intrinsic negative thermal expansion and ZTE. Figure 2 shows that we have phase coexistence of M_{PM} and M_{NTE} below T_N, then coexistence of M_{NTE} and M_{PTE}. Finally we have just the M_{PTE} phase at low T when the M_{NTE} phase abruptly collapses and transforms to the M_{PTE} phase, indicating that the transition is strongly first order. For Zn96 the sample fully transforms to the M_{NTE} phase upon cooling below 185 K, which exists over a wider temperature range before the lattice collapses and fully converts to the M_{PTE} phase. For Zn93 the sample fully transforms to the M_{NTE} phase at 185 K, which is then stable over the full temperature range below T_N. Table I also gives the refinements for the AFM M_{NTE} phase, emphasizing its extraordinary dependence on Zn vacancies. Additional crystallographic details are provided in the Supplemental Material.[31]

There are several important results revealed by the data of Fig. 1. First and most importantly, a_{NTE} is essentially independent of temperature. In particular, the coefficient of linear expansion α_{NTE} ($\Delta L/L\Delta T$) obtained directly from the diffraction data demonstrates that it is in the range of 10^{-7} K^{-1}, which is generally considered ZTE, over the full temperature range where the M_{NTE} exists. This value of α is considerably smaller and can occur over a much wider temperature range than Invar itself.[6–8] More importantly, it is clear that the Zn vacancies control which magnetic structure is formed, and over what temperature range. Finally, we see that only the magnetic structure of Fig. 1(b) is strongly coupled to the lattice to produce the large NTE that compensates the ordinary thermal expansion behavior, to produce the ZTE phase. We

TABLE I. Crystal structure obtained from NPD Rietveld refinements for the Mn_3Zn_xN compounds at 295 K (space group: $Pm\text{-}3m$) and the data for the magnetic M_{NTE} phase. Uncertainties indicate one standard deviation.

Sample No.	Zn99	Zn96	Zn93
Formula	$Mn_3Zn_{0.99}N$	$Mn_3Zn_{0.96}N$	$Mn_3Zn_{0.93}N$
A (Å)	3.90077(6)	3.90021(4)	3.89891 (1)
V (Å^3)	59.342(1)	59.309 (1)	59.282 (1)
Mn n	1.00	1.00	1.00
Zn n	0.99(1)	0.96(1)	0.93(1)
N n	0.98(2)	0.99(1)	0.99(1)
R_p (%)	5.83	7.70	6.21
R_{wp} (%)	7.54	11.24	8.59
χ^2	1.565	1.090	1.307
Zn-Mn (Å)	2.75807(1)	2.75756(1)	2.75714(1)
Mn-N (Å)	1.95025(1)	1.94989(1)	1.94959(1)
Zn-N (Å)	3.37793 (1)	3.37731(1)	3.37679(1)
	For M_{NTE} phase		
Existing temperature range	135–185 K	125–185 K	4–185 K
Fraction	83%	100%	100%
Mean lattice constant (Å)	3.9106(2)	3.9089(2)	3.9114(2)
α_l (10^{-7} K^{-1}):	8.65	− 1.37	5.83

note that Ref. 26 suggested that the large magnetovolume effect (MVE) had an intimate correlation with the cubic Γ^{5g} AF structure in $Mn_3Cu_{1-x}Ge_xN$, which can be explained in terms of geometrical frustration. This is in agreement with our experimental results in Mn_3Zn_xN, that only the magnetic phase M_{NTE} exhibits the MVE effect. This behavior may originate from the additional Zn vacancies enhancing the magnetic frustration, thereby stabilizing the M_{NTE} phase. On the other hand, Refs. 24 and 32 reported the competitive coexistence between the Γ^{5g} and Γ^{4g} antiferromagnetic components in $Mn_3Cu_{1-x}Ge_xN$ ($x = 0.5$) and suggested that the Γ^{5g} antiferromagnetic ordered moment induced by local lattice distortion is responsible for the negative thermal expansion, but guessed that the behavior was caused by slight differences in the nitrogen composition. Reference 33 observed a similar phenomenon as us in Mn_3ZnN, but they hypothesized that it was due to the disorder on N site.

The juxtaposition of the NTE and PTE phases, along with the smooth variation of the lattice parameter of the PM and PTE phases, allows a quantitative evaluation of the magnetic coupling to the lattice for the M_{NTE} phase. The behavior of this phase is a result of a competition between the expansion of the lattice upon cooling due to the magnetic ordering [$a_M(T)$] and the usual thermal contraction $a_T(T)$. For Zn99 and Zn96, $a_T(T)$ can be readily extrapolated into the regions of existence of M_{NTE} from the smooth variation of the lattice parameters a_{PM} and a_{PTE}. For Zn93 this is more difficult because of the large temperature range of M_{NTE}. We could use the same extrapolation from the PM phase, but a better estimate can be obtained by noting that $a_{PTE} < a_{NTE}$, so that applying pressure should have a dramatic effect on the phases. NPD data were then collected for the Zn93 sample at a hydrostatic pressure of 0.55 GPa, which was sufficient to fully convert M_{NTE} into M_{PTE}, or PM at higher temperature. Then a_{PM} and a_{PTE} form the usual smooth curve, as shown by the open triangles in Fig. 1(f). These data were scaled and matched to the observed a_{PM} at ambient pressure to estimate $a_T(T)$ below T_N for Zn93.

Since there is no significant coupling of the magnetic moments and the lattice in the M_{PTE} phase, we can assume that $a_{PTE}(T) = a_{PM}(T) = a_T(T)$ and take the difference $\Delta a_m(T) = a_{NTE}(T) - a_T(T)$ to isolate the effect of the NTE. The results are shown in Fig. 3. For all three compositions we see that $\Delta a_m(T)$ increases modestly with decreasing temperature, but at approximately the same rate as the ordered moment increases. We find that the ratio $r(T) = \Delta a_m(T)/m_{NTE}(T)$ is approximately independent of T, revealing that the size of the NTE effect is controlled by the size of the ordered moment. These data are shown by the solid purple squares, and fit to an offset plus a straight line are given in the figure. Note that for the Zn99 sample the M_{NTE} phase exists only over a small temperature region, and then begins to convert to the M_{PTE} phase. During this transformation the phase fraction decreases toward zero (also see Fig. 2) and it becomes difficult to extract the moment in the M_{NTE} phase, but there appears to be some decrease in its value when the two phases coexist. For the Zn96 and Zn93 samples the transformations are abrupt and no coexistence or moment decrease is observed. It is clear that strong spin-lattice coupling is responsible for the abnormal thermal expansion behavior observed in the M_{NTE} phase, with $\Delta a_m(T)$ offsetting the usual contribution of the thermal vibrations almost exactly, yielding a system with extremely small thermal expansion.

Figure 3 also shows the ordered Mn moments for the M_{PTE} phase. This phase has two inequivalent magnetic atoms with different ordered magnetic moments $m_{PTE}(T)$ and $m'_{PTE}(T)$, in agreement with Refs. 29 and 30. For the Zn99 sample both moments increase slowly with decreasing temperature [Fig. 3(a)], while they remain approximately constant for Zn96 [Fig. 3(b)]. Since there is no significant moment-lattice coupling in this M_{PTE} phase the moment values are unimportant as far as the thermal expansion is concerned.

A central result of the present study is that changes in the Zn content control the phases that occur and their temperature range of existence. This suggests that the properties can also

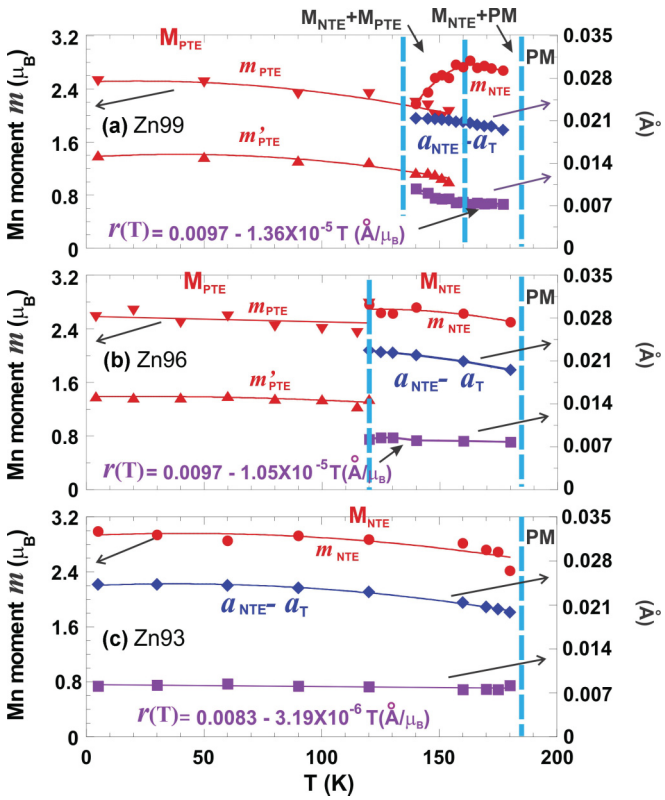

FIG. 3. (Color online) (a)–(c) Relationship between the lattice variation a_{NTE}-a_T, ordered magnetic moments, and $r(T)$ for three Zn occupancies. The data for (a) Zn99, (b) Zn96, and (c) Zn93 show that the temperature variation of the lattice parameter is proportional to the ordered magnetic moment in the M_{NTE} phase due to the presence of strong magnetoelastic coupling.

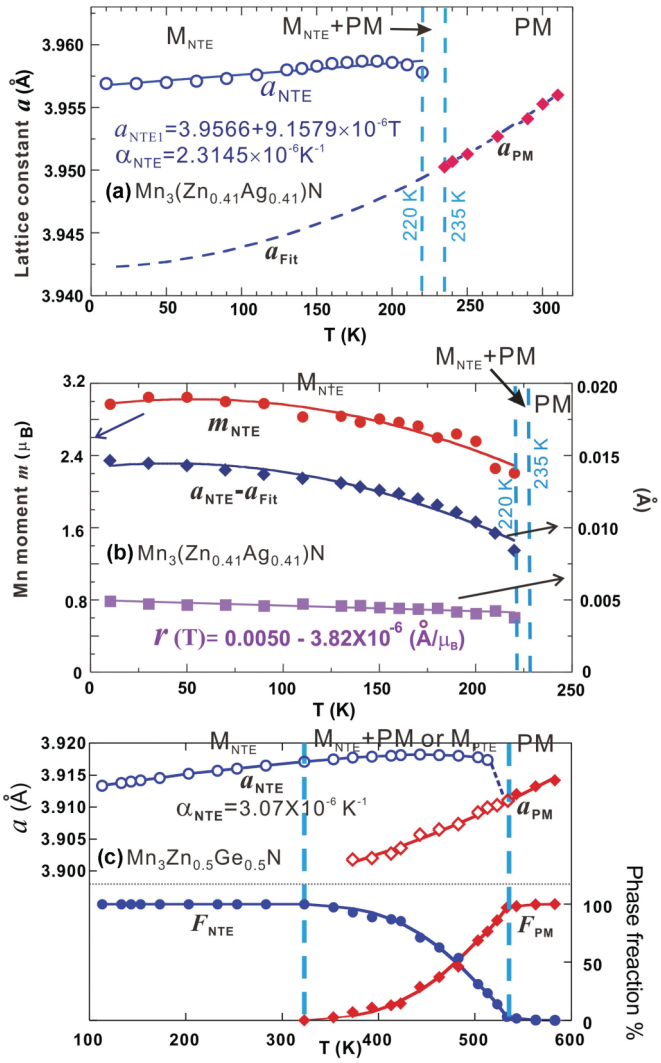

FIG. 4. (Color online) Temperature dependence of the cubic lattice parameter and ordered moment in $Mn_3Zn_{0.41}Ag_{0.41}N$ and $Mn_3Zn_{0.5}Ge_{0.5}N$. (a) shows the lattice parameter and (b) the ordered magnetic moment for $Mn_3Zn_{0.41}Ag_{0.41}N$, demonstrating the ZTE behavior, with $r(T)$ essentially constant. (c) Lattice parameter and phase fraction for $Mn_3Zn_{0.5}Ge_{0.5}N$, with an antiferromagnetic ordering temperature adjusted to 530 K.

be controlled by appropriate chemical substitution on the Zn site, which changes both the ordered magnetic moment and lattice constant, and we now show this explicitly for the $Mn_3(Zn/Ag)_{0.82}N$ and $Mn_3(Zn/Ge)N$ systems. We have prepared the compounds $Mn_3Zn_{0.41}Ag_{0.41}N$ and $Mn_3Zn_{0.5}Ge_{0.5}N$ and their thermal expansion properties are illustrated in Fig. 4 (also see Table S-II in the Supplemental Material[31]). For $Mn_3(Zn/Ag)_{0.82}N$, T_N increases to 220 K by partially replacing Zn by Ag, which has a larger ionic size [Figs. 4(a) and 4(b)], and by inducing vacancies at the Zn site to stabilize the M_{NTE} phase. A value of $\alpha = 2.31 \times 10^{-6}$ K^{-1} is obtained in the entire temperature range below T_N, measured by the variable temperature NPD technique. In the second case, with 50% of Zn replaced by Ge, T_N increases to 530 K and the M_{NTE} phase with $\alpha = 3.07 \times 10^{-6}$ K^{-1} occurs for an extended range [350–530 K, Fig. 4(c)] as determined by XRD. Reference 8 observed that stress could induce an expanded temperature region for low thermal expansion (LTE) in Invar and thought that microstrain around the Fe atoms introduced a slight increase in the Fe-Fe interatomic distances. This may be a common mechanism for the present system in correlating the micromagneto-structure and abnormal thermal expansion.

The results presented here elucidate how NTE for these cubic antiperovskite systems is intimately correlated with the magnetic structure and can be tuned by adjusting the chemical and vacancy concentrations to work from well below to well above room temperature. We have shown how to stabilize the M_{NTE} phase, adjust the magnetic ordering temperature and ordered magnetic moment to achieve ZTE, and have provided a quantitative relationship between the ordered magnetic moment and lattice variation that controls the ZTE mechanism. The tools developed here can be readily employed to tune the thermal expansion properties, including compensating for metallurgical defects such as grain boundaries or impurities if required, to the temperature range and breadth required for a wide variety of real world applications.

Work in China was supported by National Natural Science Foundation of China (NSFC) (No. 51172012 and No. 91122026). The authors thank D. A. Neumann and A. Santoro (NIST) for very constructive discussions.

*congwang@buaa.edu.cn
†jeffrey.lynn@nist.gov

[1]H. Akitaya *et al*., Proc. SPIE **7018**, 70183H (2008).
[2]J. D. Strock, Proc. SPIE **1690**, 223 (1992).
[3]C. F. Grimsey Jr., US Patent No. 3077958 (19 Feb. 1963).
[4]J. Sugawara, H. Unno, and N. Kosugi, in HEAT Technical Committee Open Symposium No. 6, Japan Society for Abrasive Technology (JSAT), 2008 (unpublished).
[5]D. A. Fleming, S. W. Johnson, and P. J. Lemaire, US Patent No. 5694503 (2 Dec. 1997).
[6]C. E. Guillaume, C. R. Acad. Sci. **125**, 235 (1897).
[7]M. Schilfgaarde, I. A. Abrikosov, and B. Johansson, Nature (London) **400**, 46 (1999).
[8]P. Gorria *et al*., Phys. Rev. B **80**, 064421 (2009).
[9]A. W. Sleight, Nature (London) **425**, 674 (2003).
[10]G. D. Barrera, J. A. O. Bruno, T. H. K. Barron, and N. L. Allan, J. Phys.: Condens. Matter **17**, R217 (2005).
[11]J. N. Grima, Proc. R. Soc. A **463**, 1585 (2007).
[12]M. Azuma *et al*., Nat. Commun. **2**, 347 (2011).
[13]J. R. Salvador, F. Guo, T. Hogan, and M. G. Kanatzidis, Nature (London) **425**, 702 (2003).
[14]W. Miller, C. W. Smith, D. S. Mackenzie, and K. E. Evans, J. Mater. Sci. **44**, 5441 (2009).
[15]T. A. Mary, J. S. O. Evans, T. Vogt, and A. W. Sleight, Science **272**, 90 (1996).
[16]X. G. Zheng, H. Kubozono, H. Yamada, K. Kato, Y. Ishiwata, and C. N. Xu, Nature (London) **3**, 724 (2008).
[17]R. Roy and D. Agrawal, Nature (London) **388**, 433 (1997).
[18]J. Chen, X. R. Xing, C. Sun, P. H. Hu, R. B. Yu, X. W. Wang, and L. H. Li, J. Am. Chem. Soc. **130**, 1144 (2008).
[19]K. Nakajima, T. Nakajima, N. Kawasaki, and Y. Owari, Proc. SPIE **5868**, 58680T (2005).
[20]Y. Sun, C. Wang, Y. C. Wen, K. G. Zhu, and J. T. Zhao, Appl. Phys. Lett. **91**, 231913 (2007).
[21]W. S. Kim, E. O. Chi, J. C. Kim, N. H. Hur, K. W. Lee, and Y. N. Choi, Phys. Rev. B **68**, 172402 (2003).
[22]K. Takenaka and H. Takagi, Appl. Phys. Lett. **94**, 131904 (2009); **87**, 261902 (2005).
[23]X. Y. Song, Z. H. Sun, Q. Z. Huang, M. Rettenmayr, X. M. Liu, M. Seyring, G. N. Li, G. H. Rao, and F. X. Yin, Adv. Mater. **23**, 4690 (2011).
[24]S. Iikubo, K. Kodama, K. Takenaka, H. Takagi, M. Takigawa, and S. Shamoto, Phys. Rev. Lett. **101**, 205901 (2008).
[25]K. Takenaka, K. Asano, M. Misawa, and H. Takagi, Appl. Phys. Lett. **92**, 011927 (2008).
[26]S. Iikubo, K. Kodama, K. Takenaka, H. Takagi, and S. Shamoto, Phys. Rev. B **77**, 020409 (2008).
[27]R. Huang, L. Li, F. Cai, X. Xu, and L. Qiang, Appl. Phys. Lett. **93**, 081902 (2008).
[28]K. Asana, K. Koyama, and K. Takenaka, Appl. Phys. Lett. **92**, 161909 (2008).
[29]D. Fruchart, E. F. Bertaut, R. Madar, and R. Fruchart, J. Phys. (Paris) **32**, C1-876 (1971).
[30]D. Fruchart and E. F. Bertaut, J. Phys. Soc. Jpn. **44**, 781 (1978).
[31]See Supplemental Material at http://link.aps.org/supplemental/10.1103/PhysRevB.85.220103 for Crystallograhic refinement results are given in the Tables S-I through S-V, together with typical refinement data (Fig. S-I) and data demonstrating coexisting phase fractions (Fig. S-II).
[32]K. Kodama, S. Iikubo, K. Takenaka, M. Takigawa, H. Takagi, and S. Shamoto, Phys. Rev. B **81**, 224419 (2010).
[33]T. Hamada and K. Takenaka, J. Appl. Phys. **111**, 07A904 (2012).